Available online at www.sciencedirect.com
SCIENCE DIRECT
International Journal of Heat and Fluid Flow 27 (2006) 522–530
International Journal of HEAT AND FLUID FLOW
www.elsevier.com/locate/ijhff

Investigations of flow characteristics in a plate fin and tube heat exchanger model composed of single cylinder

B. Şahin [a,*], A. Akkoca [b], N.A. Öztürk [a], H. Akilli [a]

[a] Department of Mechanical Engineering, Cukurova University, 01330 Adana, Turkey
[b] Department of Mechanical Engineering, Mersin University, 33342 Mersin, Turkey

Received 22 December 2004; received in revised form 14 November 2005; accepted 18 November 2005
Available online 14 February 2006

Abstract

The flow structure in a plate fin and tube heat exchanger model composed of single cylinder located between two parallel plates for duct height-to-cylinder diameter ratio of 0.365 for Reynolds numbers of 4000 and 7500 is investigated experimentally. Particle image velocimetry (PIV) technique is employed to obtain instantaneous, time-averaged and phase-averaged turbulent flow characteristics in the heat exchanger flow passage. Interactions between the main flow and the secondary flow are examined in detail in the horizontal and vertical planes of the flow passage. Horseshoe vortex system formed in close region of cylinder–plate junction and convected downstream in the main flow direction and its evolution in the circumference of the cylinder is also investigated in detail.

Keywords: PIV; Horseshoe vortex; Plate fin and tube heat exchanger; Turbulent flow

1. Introduction

In the present investigation, the attention is focused on a compact, single phase, plate fin and tube heat exchanger having continuous plain fins that is attached perpendicularly to the outside of the circular tubes. These types of heat exchangers are very common in space heating and/or cooling devices such as in air conditioning units, fan-coils, unit heaters, and radiators, in condensers and evaporators, and in heat recovery systems. The fins on the outside of the tubes are used to obtain high heat transfer performance surfaces. In industry, among wavy, slit, and louvered fin configurations, mostly plain fin configurations are preferred because of their long term operation, simplicity, and lower friction characteristics. Therefore, in this study, a heat exchanger model comprised of a circular cylinder located between two parallel plates representing a compact heat exchanger is prepared in order to investigate the flow characteristics occurring in the heat exchanger flow passage in detail.

The flow characteristics in the heat exchanger flow passage are strongly affected by the presence of both cylinders and fin plates. Flow of fluid between adjacent fins and around the tube results in a complex three-dimensional flow and increased heat transfer performance. Heat transfer problem in the heat exchangers is strongly related to the flow structure. The complex flow structure includes developing velocity and thermal boundary layers beginning from the leading edges of the fins and over the tubes; continuous creation, destruction, separation and reattachment of new boundary layers due to the existence of tubes; formation of horseshoe vortices in front of the tubes; extending of horseshoe vortices to the rear of the tubes; recirculating tube wakes; vortex shedding in the wake of both tubes and fins. Horseshoe vortices can be seen at any time—a boundary layer encounters a wall mounted bluff body and is very important in various engineering applications. In the heat exchangers, as the flow approaches to the tubes, the horseshoe vortex system forms

* Corresponding author. Tel.: +90 322 3387063; fax: +90 322 3386126.
E-mail address: bsahin@cu.edu.tr (B. Şahin).

0142-727X/$ - see front matter © 2005 Elsevier Inc. All rights reserved.
doi:10.1016/j.ijheatfluidflow.2005.11.005

Nomenclature

D	cylinder diameter	u'	fluctuations of u
F	center of focus	v'	mean fluctuations of v
F_s	distance between two plates	u_{rms}	root mean square of u
Re	Reynolds number	v_{rms}	root mean square of v
S	saddle point	U	free stream velocity
u	streamwise velocity component	V	velocity vector
v	transverse velocity component	ψ	streamline
$u'v'$	Reynolds stress	ω	vorticity

in front of each tube in the stagnation area near the tube and the fin junction region. The existence of horseshoe vortices introduce additional mixing of hot and cold fluids in the heat exchanger flow passage and consequently increase the fin heat transfer in that area. Time-evolution of horseshoe vortices in the vicinity of the cylinder surface and a detailed flow structure influencing the heat transfer coefficient in the heat exchanger flow passage are examined in detail by Tutar and Akkoca (2004).

There are a number of experimental studies in the literature regarding flow and heat transfer characteristics of these types of heat exchangers. Saboya and Sparrow (1974), Goldstein and Sparrow (1976), Rocha et al. (1997), and Kim and Song (2002, 2003) used naphthalene sublimation technique in order to measure local heat and mass transfer coefficients on the fin surface and around the tube. They examined a main and a subsidiary horseshoe vortex formed in front of the tube extending their trail along the side of the tube causing a substantial increase in total heat and mass transfer rates. They obtained low heat and mass transfer coefficients in the wake region downstream of the tube. Critoph et al. (1999) and Wierbowski and Stasiek (2002) used thermochromic liquid crystal technique to measure local heat transfer coefficients, local air temperatures, and velocity distributions in heat exchangers. Seshimo and Fujii (1991), Jang et al. (1996, 1998), Valencia et al. (1996), Wang et al. (1997, 1998, 1999a,b), Madi et al. (1998), Yan and Sheen (2000), Halici et al. (2001), Lozza and Merlo (2001), and Ay et al. (2002) performed wind tunnel experiments to investigate effects of different geometrical parameters on the heat transfer, pressure drop, and the performance of heat exchangers. Kundu et al. (1992) measured heat transfer and pressure drop in the heat exchanger for laminar and turbulent flow and defined a criterion for transition from laminar to turbulent flow. Mendez et al. (2000) examined the effect of fin spacing on a single cylinder heat exchanger through dye injection technique and showed that the horseshoe vortex development depends on the fin spacing and Reynolds number and corresponds to the peak in the Nusselt number. Akkoca (2004) carried out an experimental and a numerical work to report detailed instantaneous and averaged flow structures including streamlines, velocity vectors, vorticity contours and horseshoe vortices formed in the heat exchanger flow passage.

In the literature, most of the studies focus on the determination of time-averaged heat and/or mass transfer coefficients and effects of geometrical parameters on heat transfer and pressure drop performance of heat exchangers under laminar flow conditions. However, it is known that flows in the heat exchanger passage have unsteady, turbulent, and 3-D flow characteristics as also reported by Zdravitsch et al. (1994), Shah et al. (1997) and Tutar and Akkoca (2004). A deeper physical understanding of local flow structure in the heat exchanger flow passage is very important for design and optimization purposes. According to the author's knowledge, limited investigations were done on the local turbulent flow structure as well as time-dependent formation and evolution of horseshoe vortex mechanism for plate fin and tube heat exchangers by using particle image velocimetry (PIV) technique. It is well known that PIV technique can be well adapted to study of turbulent flows and give quantitative information on the spatial structure of the velocity field. Therefore, the PIV technique is employed to obtain instantaneous spatial turbulent velocity field and calculate instantaneous and averaged turbulence quantities in the heat exchanger flow passage to understand local flow characteristics at various Reynolds numbers for duct height-to-cylinder diameter ratio of 0.365.

2. Experimental study

2.1. Experimental system and measurement technique

Experiments were performed at Mechanical Engineering Department at Çukurova University, Turkey. The experimental set-up comprised of a closed loop open surface water channel having dimensions of $8000 \times 1000 \times 750$ mm made from 15 mm thick transparent plexiglass sheet. Before reaching the test chamber, the water was pumped into a settling chamber and passed through a honeycomb section and a two-to-one channel contraction. Water pump is driven by an electric motor with a variable speed controller. The depth of the water in the test section was adjusted to 650 mm height for the present experiments.

A schematic of the test chamber used in the present experiment is shown in Fig. 1. The test section consists of

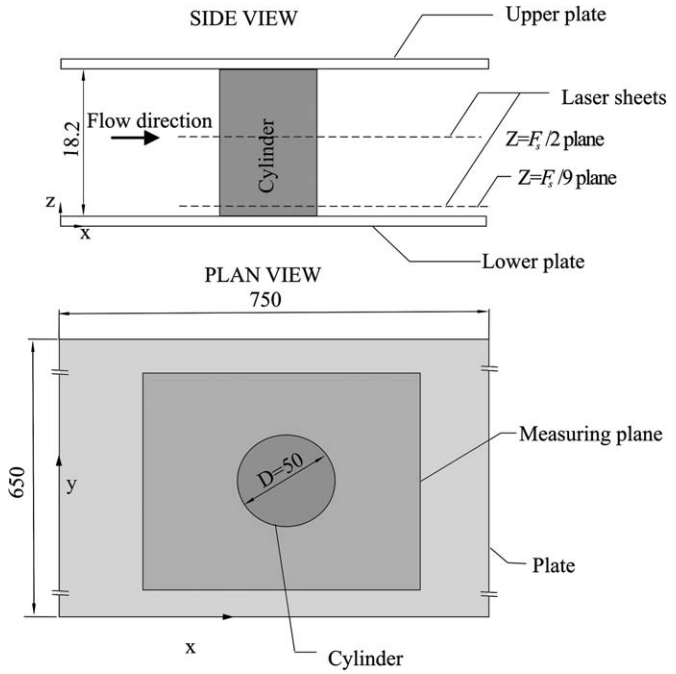

Fig. 1. Schematic representation of laser sheets, plan and side views of test section (all dimensions are in mm).

a cylinder attached to the lower plate and mechanically press fitted to the upper plate. The cylinder and the plates are made from plexiglass material so that the laser light propogates easily from the plates and the cylinder. The cylinder outer diameter and the fin length are 50 mm and 750 mm, respectively. Experiments are conducted for fin spacing to cylinder diameter ratio of 0.365 which is sufficient for horseshoe vortices to form and contribute to the increase of heat transfer rate as reported by Tutar and Akkoca (2004). To avoid flow disturbances that may occur in the heat exchanger flow passage, the leading edge of the plates are specially beveled as well as the width and the length of the plates are extended 6 and 7 times the tube diameter in longitudinal and transverse directions both upstream and downstream of the cylinder. Before beginning the experiments, flow structure around the cylinder and the plate junction regions is examined in detail using dye injection and no external flow disturbances are observed.

The instantaneous velocity field in the heat exchanger flow passage is measured and the data is recorded using Dantec PIV system and Flow Manager software. The measurement field is enlightened by using a pair of double-pulsed Nd:YAG laser units. Each laser produces a thin and intensed green light sheet. The velocity vector analysis is performed by recording the locations of the particles throughout the two-dimensional area of the flow and obtaining the change in position of the particles between the two pulses and the time-interval between the pulses. A cross-correlation CCD camera with a resolution of 1016×1016 pixels is used to capture the particle images. An input buffer is used to read and store the image maps from the CCD camera. To transfer the images from the camera to the computer, a high-speed digital frame grabber is employed. To capture the flow field images, the laser pulse and camera must be triggered with the correct sequence and timing. Therefore, a synchronizer is used to control all of the components, which are initiated at the exact moment necessary. These captured images are recorded into the memory of a personal computer. Two hundred frames are recorded successively for one series of image capturing. The area of the full frame of plan view and side view images are 170×170 mm^2 and 88×18.2 mm^2 respectively.

Before the image processing, spurious vectors are detected and removed as well as the digital images were improved and smoothed by neighborhood averaging technique. The uncertainty of the velocity vectors of the present study is estimated as less than 2%.

2.2. Experimental results and discussion

Understanding of flow details in the heat exchanger flow passage is important in terms of design and optimization of heat exchangers. In order to reveal the flow details, velocity vector maps, patterns of streamline, vorticity contours, Reynolds stress contours, and root mean square of velocity components are presented. Time-averaged flow data are obtained by averaging of 200 PIV images.

Fig. 2 presents time-averaged velocity vector map $\langle V \rangle$, corresponding streamline pattern $\langle \psi \rangle$, vorticity contours $\langle \omega \rangle$, contours of normalized Reynolds stress $\langle u'v' \rangle / U^2$, and contours of normalized root mean square of streamwise and transverse velocity fluctuations, u_{rms}/U and v_{rms}/U, inside the flow passage close to the lower plate at $Z = F_s/9$ plane for $Re = 4000$ based on the cylinder diameter ($D = 50$ mm) having free stream velocity of $U = 8$ cm/s. Here, U is the free stream velocity, u_{rms} and v_{rms} are root mean square of the streamwise, u, and transverse, v, velocity components, respectively. As it is clearly seen from the velocity vector map shown in Fig. 2a, relatively wider and longer wake region occurs downstream of the cylinder. The corresponding streamline patterns reveal that two symmetrical foci with opposite circulation and a saddle point behind them are evident. The centers of the foci and the saddle point are designated as F and S as indicated in Fig. 2b, respectively. In Fig. 2c, symmetrically distributed cluster of positive (solid line) and negative (dashed line) vorticity layers beginning from the vicinity of stagnation point in front of the cylinder and extending further downstream around the plane of symmetry of the cylinder are evident. In addition, three neighboring layers of relatively weaker vorticities surrounding the positive and negative vorticity clusters each located outside of the shear layer are observed. The corresponding normalized Reynolds stress contours ($\langle u'v' \rangle / U^2$, where u' and v' are fluctuations of u and v, respectively) are shown in Fig. 2d. The peak values of positive and negative Reynolds stress contours indicate regions under high fluctuations. These regions are located far downstream of

the cylinder where shear layers and shedding vortices emerging on both sides of the cylinder interact each other as well as immediately adjacent to the upstream surface of the cylinder and along the outer side of the shear layer. The turbulent flow characteristics are also presented in terms of root mean square values of streamwise velocity, u, (u_{rms}) and transverse velocity, v, (v_{rms}) in order to identify regions of high fluctuations as shown in Fig. 2e and f, respectively. Both u_{rms} and v_{rms} are normalized by free stream velocity U. High concentrations of u_{rms}/U contours are located in the proximity of upper surface of the cylinder along the shear layer and downstream of concentrated vortices. It is clearly seen that v_{rms}/U contours are stacked far downstream of the cylinder as well as in the proximity of upper surface of the cylinder at both sides as seen in Fig. 2f. Peaks values of u_{rms}/U and v_{rms}/U are 0.43 and 0.60, respectively. The highest amplitude of v_{rms}/U appears immediately adjacent to the downstream side of the saddle point. The minimum and incremental values of vorticity, normalized Reynolds stress, and normalized root mean square of streamwise and transverse velocity fluctuations are given in the figure captions.

Fig. 3 illustrates time-averaged velocity vector map, patterns of streamline, vorticity contours, normalized Reynolds stress contours, and contours of u_{rms}/U and v_{rms}/U at $Z = F_s/9$ plane for $Re = 7500$ based on the cylinder

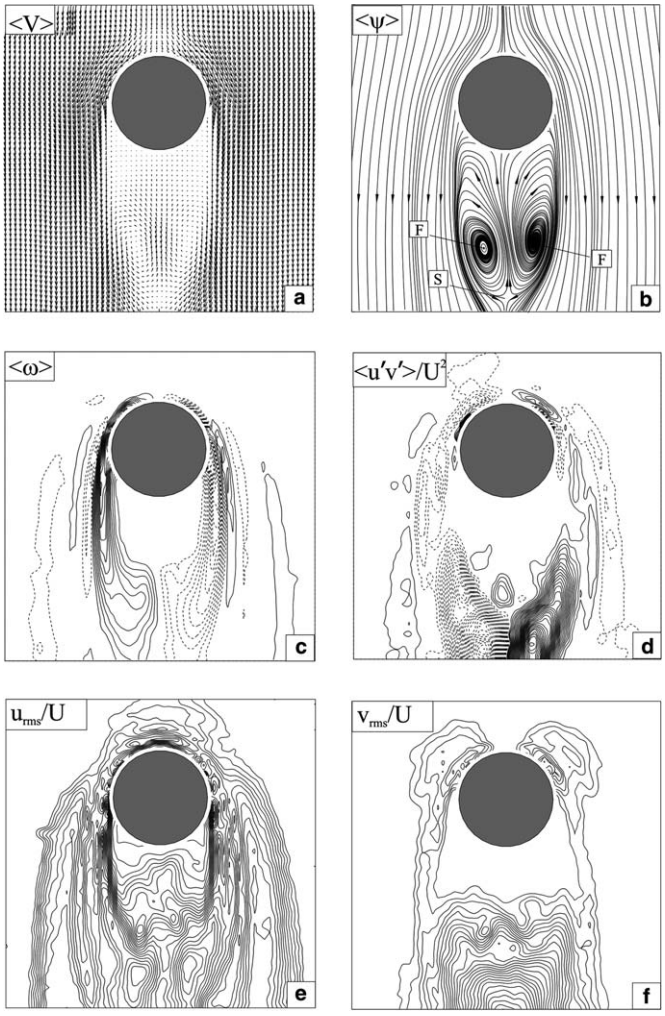

Fig. 2. Time-averaged flow data at $Z = F_s/9$ plane for $Re = 4000$. (a) Velocity vector map, (b) streamline pattern, (c) vorticity contours, (d) normalized Reynolds stress contours, (e) contours of normalized root mean square of streamwise velocity fluctuations, (f) contours of normalized root mean square of transverse velocity fluctuations. The minimum and incremental values of vorticity are $\omega_{\min} = \pm 1\ \mathrm{s}^{-1}$ and $\Delta\omega = 1\ \mathrm{s}^{-1}$. The minimum and incremental values of normalized Reynolds stress are $[\langle u'v'\rangle/U^2]_{\min} = \pm 0.004$ and $\Delta[\langle u'v'\rangle/U^2] = 0.004$. The minimum and incremental values of normalized root mean square of streamwise and transverse velocity fluctuations are $[u_{\mathrm{rms}}/U]_{\min} = [v_{\mathrm{rms}}/U]_{\min} = 0.02$ and $\Delta[u_{\mathrm{rms}}/U] = \Delta[v_{\mathrm{rms}}/U] = 0.02$.

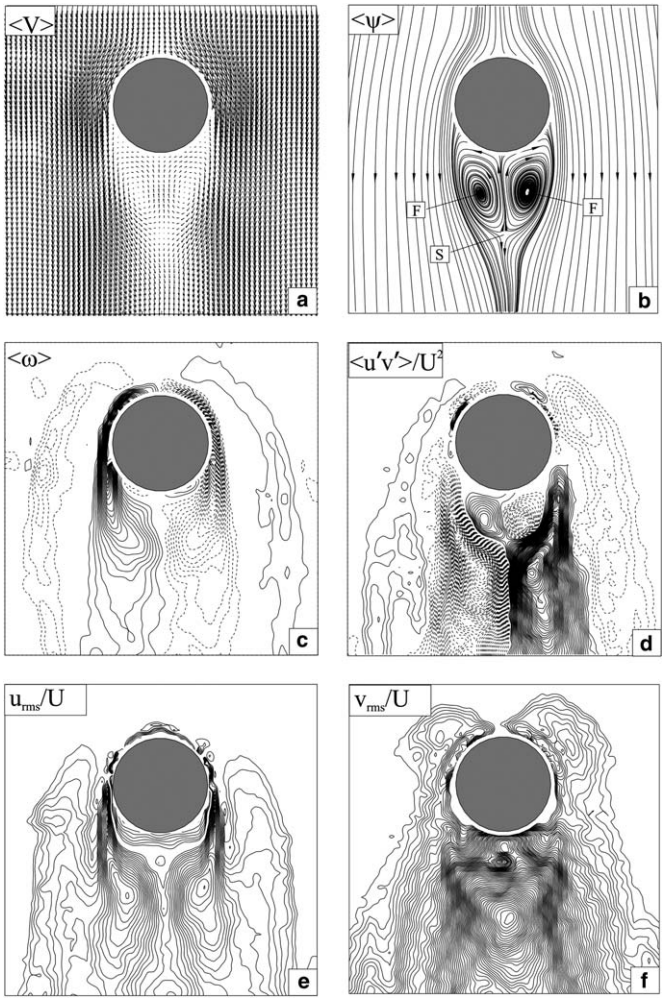

Fig. 3. Time-averaged flow data at $Z = F_s/9$ plane for $Re = 7500$. (a) Velocity vector map, (b) streamline pattern, (c) vorticity contours, (d) normalized Reynolds stress contours, (e) contours of normalized root mean square of streamwise velocity fluctuations, (f) contours of normalized root mean square of transverse velocity fluctuations. The minimum and incremental values of vorticity are $\omega_{\min} = \pm 1\ \mathrm{s}^{-1}$ and $\Delta\omega = 1\ \mathrm{s}^{-1}$. The minimum and incremental values of normalized Reynolds stress are $[\langle u'v'\rangle/U^2]_{\min} = \pm 0.004$ and $\Delta[\langle u'v'\rangle/U^2] = 0.004$. The minimum and incremental values of normalized root mean square of streamwise and transverse velocity fluctuations are $[u_{\mathrm{rms}}/U]_{\min} = [v_{\mathrm{rms}}/U]_{\min} = 0.02$ and $\Delta[u_{\mathrm{rms}}/U] = \Delta[v_{\mathrm{rms}}/U] = 0.02$.

diameter ($D = 50$ mm) having free stream velocity of $U = 15$ cm/s. As it is clearly seen in Fig. 3a, the size of the reversed flow region downstream of the cylinder becomes smaller as well as the centers of the recirculating zone shift towards the cylinder surface as the Reynolds number is increased from 4000 to 7500. Similarly, positions of the center of two symmetric foci and the saddle point shift towards the cylinder surface as the Reynolds number is increased as shown in Figs. 2b and 3b. As seen in Fig. 3c, more compact, stronger, and symmetrically distributed positive and negative vorticity clusters beginning from the vicinity of stagnation point in the upper region of the cylinder surface and convecting further downstream around the plane of symmetry are observed comparing to the results presented in Fig. 2c. In addition to symmetrically distributed cluster of vorticities, a pair of vorticity layer exterior to the shear layer is also observed. Though their origins were not clear in the case of $Re = 4000$, it is evident that in Fig. 3c these vorticity layers originate in close proximity to the upstream of the cylinder–plate junction. The vortices observed on the outer part of the shear layer are so-called horseshoe vortices. In Fig. 3d, stronger patterns of Reynolds stresses are obtained comparing to Fig. 2d due an increase in Reynolds number. It is clear that in the case of $Re = 7500$, higher concentrations of Reynolds stress are obtained downstream of the cylinder and along the both sides of the separating shear layers compared with the case of $Re = 4000$. The locations of the centers of high concentration of the Reynolds stress contours where the highest turbulence activities occur are displaced towards the cylinder in the wake region, and also outer side of the shear layers. A relatively low level of fluctuations of Reynolds stress which occupy the outer regions of shear layers may be caused by the horseshoe vortices. The turbulent flow characteristics in the flow passage of the heat exchanger are also presented in terms of root mean square values of streamwise velocity, u, (u_{rms}/U) and transverse velocity, v, (v_{rms}/U) components. It is observed that u_{rms}/U and v_{rms}/U contours occupy a larger extent of the flow domain indicating higher level of fluctuations with $Re = 7500$ as seen in Fig. 3e and f. Large amplitudes of u_{rms}/U and v_{rms}/U appear immediately adjacent to the cylinder base in the case of $Re = 7500$ comparing to the case of $Re = 4000$. The peak values of u_{rms}/U and v_{rms}/U are 0.58 and 0.78, respectively. In addition, the maximum value of u_{rms}/U occurs on both sides of the saddle point, whereas the maximum values of v_{rms}/U occurs at the center of the saddle point.

Fig. 4 illustrates time-averaged flow data at mid-plane of the flow passage at $Z = F_s/2$ for $Re = 4000$ and 7500. As the Reynolds number is increased from 4000 to 7500, the size of the wake region becomes smaller, relatively wider vorticity clusters around the plane of symmetry of the cylinder forms, the locations of the peak values of the normalized Reynolds stress shift towards the cylinder surface, and more compact and stronger u_{rms}/U and v_{rms}/U contours arise. In addition to these flow features obtained at the mid-plane of the flow passage ($Z = F_s/2$), comparison of Figs. 2–4 reveals that some different flow characteristics are also observed such as horseshoe vortex system and higher strength of the turbulence quantities occur at $Z = F_s/9$ plane. On the other hand, there is no clear evi-

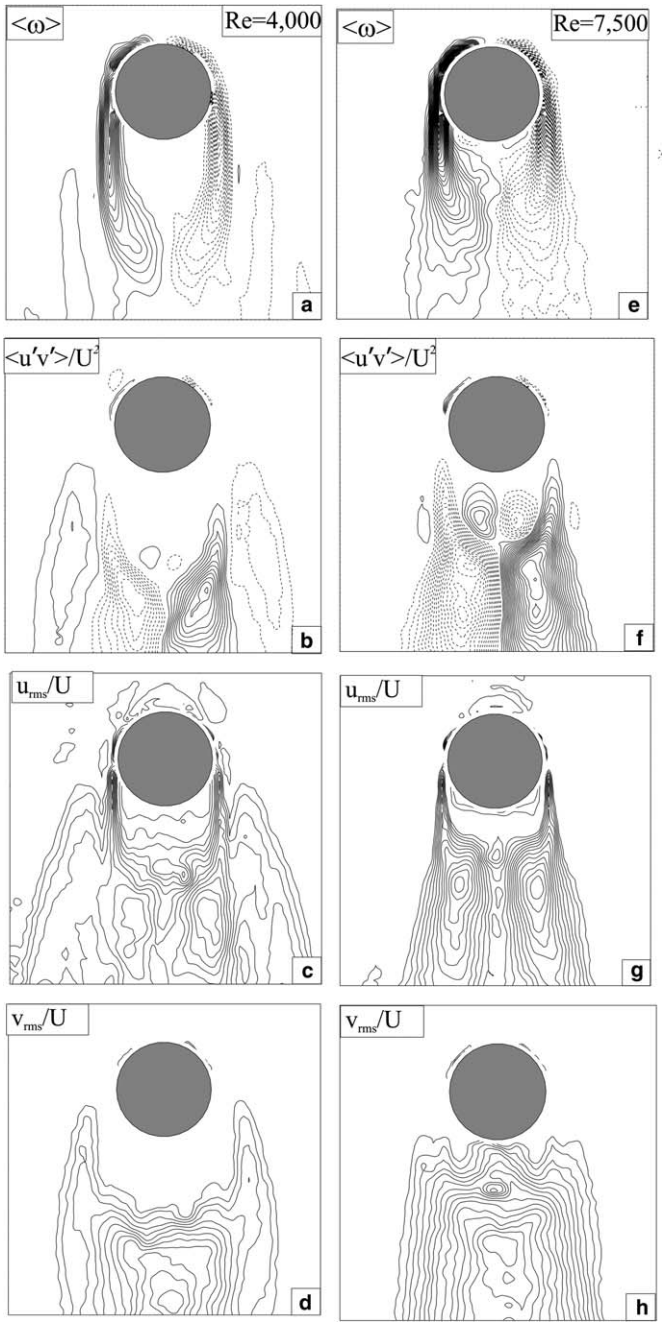

Fig. 4. Time-averaged flow data at $Z = F_s/2$ plane for $Re = 4000$ and $Re = 7500$. (a,e) Vorticity contours, (b,f) normalized Reynolds stress contours, (c,g) contours of normalized root mean square of streamwise velocity fluctuations, (d,h) contours of normalized root mean square of transverse velocity fluctuations. The minimum and incremental values of vorticity are $\omega_{\min} = \pm 1\ \mathrm{s}^{-1}$ and $\Delta\omega = 1\ \mathrm{s}^{-1}$. The minimum and incremental values of normalized Reynolds stress are $[\langle u'v'\rangle/U^2]_{\min} = \pm 0.004$ and $\Delta[\langle u'v'\rangle/U^2] = 0.004$. The minimum and incremental values of normalized root mean square of streamwise and transverse velocity fluctuations are $[u_{\mathrm{rms}}/U]_{\min} = [v_{\mathrm{rms}}/U]_{\min} = 0.02$ and $\Delta[u_{\mathrm{rms}}/U] = \Delta[v_{\mathrm{rms}}/U] = 0.02$.

dence for horseshoe vortex formation due to that the flow is not affected so much by the presence of the fin plates at the mid-plane of the flow passage $Z = F_s/2$, as shown in Fig. 4. In addition, relatively weaker concentrations of turbulence quantities are observed in this plane comparing to the results obtained at $Z = F_s/9$ plane. It is also evident that $\langle u'v' \rangle / U^2$, u_{rms}/U and v_{rms}/U contours are stacked downstream of the cylinder instead of being spread in the entire flow domain as shown in Fig. 4. Therefore, it is concluded that more instability and mixing of the fluid,

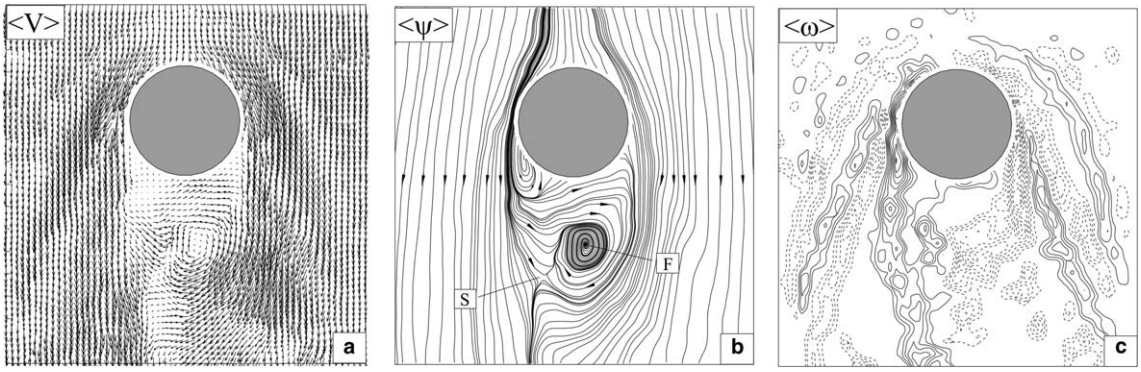

Fig. 5. Instantaneous flow data at $Z = F_s/9$ plane for $Re = 7500$. (a) Velocity vector map, (b) streamline pattern, (c) vorticity contours. The minimum and incremental values of vorticity are $\omega_{min} = \pm 3\ s^{-1}$ and $\Delta\omega = 1.5\ s^{-1}$.

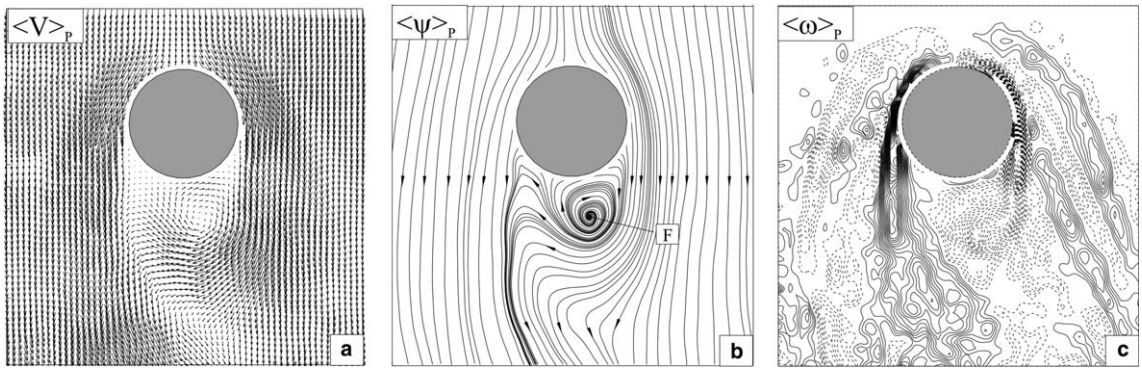

Fig. 6. Phase-averaged flow data at $Z = F_s/9$ plane for $Re = 7500$. (a) Velocity vector map, (b) streamline pattern, (c) vorticity contours. The minimum and incremental values of vorticity are $\omega_{min} = \pm 3\ s^{-1}$ and $\Delta\omega = 1.5\ s^{-1}$.

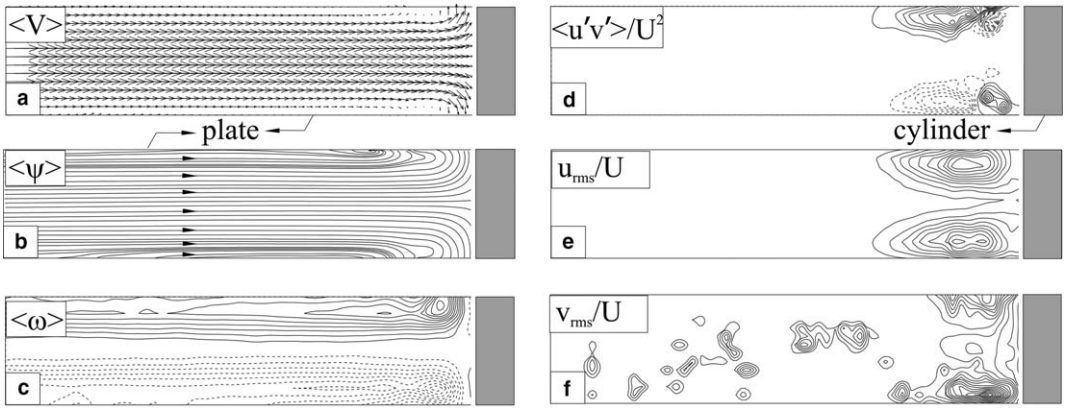

Fig. 7. Time-averaged flow data for $Re = 4000$. (a) Velocity vector map, (b) streamline pattern, (c) vorticity contours, (d) normalized Reynolds stress contours, (e) contours of normalized root mean square of streamwise velocity fluctuations, (f) contours of normalized root mean square of transverse velocity fluctuations. The minimum and incremental values of vorticity are $\omega_{min} = \pm 3\ s^{-1}$ and $\Delta\omega = 3\ s^{-1}$. The minimum and incremental values of normalized Reynolds stress are $[\langle u'v' \rangle / U^2]_{min} = \pm 0.001$ and $\Delta[\langle u'v' \rangle / U^2] = 0.001$. The minimum and incremental values of normalized root mean square of streamwise and transverse velocity fluctuations are $[u_{rms}/U]_{min} = [v_{rms}/U]_{min} = 0.02$ and $\Delta[u_{rms}/U] = \Delta[v_{rms}/U] = 0.02$.

stronger concentrations of vorticity and Reynolds stresses, and increased velocity fluctuations occur at $Z = F_s/9$ plane compared with the data obtained at the mid-plane of the flow passage $Z = F_s/2$.

Fig. 5 demonstrates the instantaneous flow patterns that measured at ($Z = F_s/9$) plane for $Re = 7500$. Unsteady wake flow behavior is clearly observed through the distributions of velocity vector and streamlines patterns presented in Fig. 5a–c. In the wake region, a strong focus is detected at $Z = F_s/9$ plane, as clearly seen in Fig. 5b. Multiple layers of positive and negative vorticity of the horseshoe vortex system occurs on both sides of the cylinder extending further downstream in the flow direction as indicated in Fig. 5c. Instantaneous pattern of streamlines presented in Fig. 5b indicates that a saddle point is clearly identifiable. Through cinema sequences, it was observed that the saddle point moves forward and backward in the streamwise direction. All instantaneous images of Fig. 5 reveal that significant variations happen in the wake region, along the outer side of the shear layer and in regions where horseshoe vortex system occurs.

In addition to time-averaged and instantaneous flow data, phase-averaged data also provides detailed information about structure of the flow field. The time history of development of the flow structure at mid and lower planes is determined from sequence of instantaneous images of velocity map. The period of repeating instantaneous images is determined using fast Fourier transformation (FFT) analysis and natural frequency spectrum. The accuracy of the selected period is controlled by examining movies of the vorticity contours. After that, a total of 8 repeating images are selected and averaged in order to determine the phase-averaged flow data at the plane close to the fin plate, at $Z = F_s/9$, for $Re = 7500$ as presented in Fig. 6. At $Re = 7500$, instabilities and unsteadiness in the wake of the cylinder are clearly seen. A strong focus

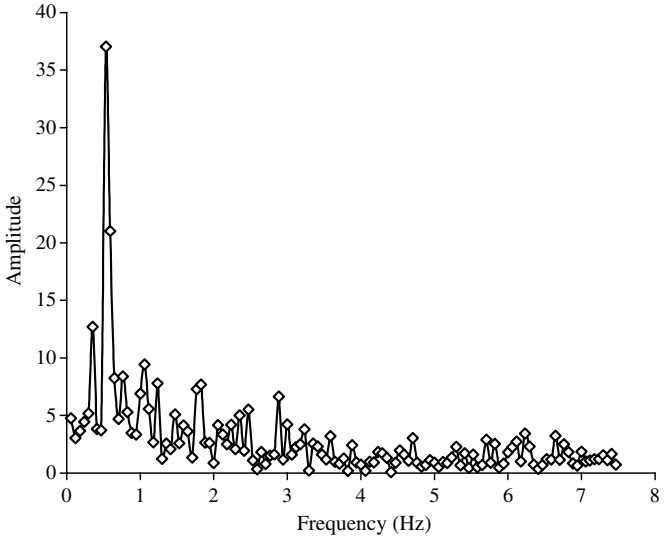

Fig. 8. Natural frequency spectrum at $Z = F_s/9$ for $Re = 7500$.

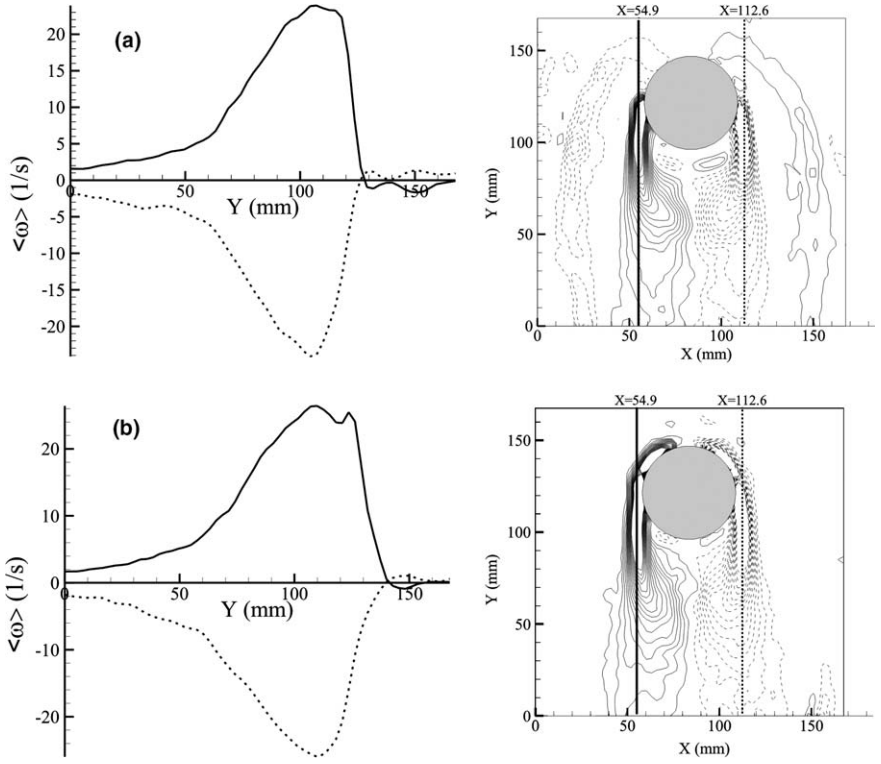

Fig. 9. Variation of time-averaged vorticity along lines corresponding to the maximum positive and negative vorticity for $Re = 7500$: (a) $Z = F_s/9$ plane and (b) $Z = F_s/2$ plane.

close to the cylinder base is clearly visible in Fig. 6b. Two pairs of strong positive and negative vorticity of horseshoe vortex systems are detected adjacent to the outer region of the shear layer.

In addition to the plan view of the images shown in Figs. 2–6, side view of the images are also illustrated as shown in Fig. 7, in order to reveal further information about the structure of the horseshoe vortex system formed in the vicinity of the cylinder–plate junction in the heat exchanger flow passage. Fig. 7 presents time-averaged flow data in side view of flow passage for $Re = 4000$. It is evident from Fig. 7a–c that, as the flow approaches the cylinder surface, it rolls up, hits the upper and lower plates and forms a pair of counter rotating vortices placed at the base of upper and lower fin plates near the cylinder–plate junction. In Fig. 7a, the velocity vectors are parallel to each other in the central region of the channel indicating a uniform incoming flow exists. The time-averaged flow data shown in Fig. 7d–f indicates that turbulent activities are concentrated in front of the cylinder near the base of the upper and lower fin plates. In other words, these counter-rotating vortices cause fluctuations and mixing of the fluid near the cylinder–plate junction.

Fig. 8 shows natural frequency spectrum of the entire flow region for 200 images at $Re = 7500$ at $Z = F_s/9$ plane. The FFT analysis is made to determine the peak of the frequency. The dominant frequency of the vortex shedding is found to be 0.529 Hz.

Fig. 9 presents the variation of the time-averaged vorticity along the specified lines corresponding to the central lines of positive and negative vortices in the longitudinal directions. These lines cross entire images starting from the bottom boundary until the top boundary. All images indicate that approximately at the same points, time-averaged vorticity get the peak values and then rapidly decrease to a certain extent for negative and positive vortices. The numerical values of positive and negative vortices along the specified lines are mostly identical.

3. Conclusion

In the present study, the characteristics of turbulent flow field in the flow passage of a heat exchanger comprised of two parallel plates and a cylinder located between the plates was investigated experimentally. The flow characteristics in the heat exchanger flow passage are highly three-dimensional and strongly affected by presence of both the cylinder and the fin plates. The relationship between flow structure and turbulence quantities are presented in terms of instantaneous, time-averaged and phase-averaged flow patterns for Reynolds numbers of $Re = 4000$ and $Re = 7500$. It is shown that structure of the turbulent flow, size of the wake region, location of singular points, position of the peak values of turbulence quantities such as concentration of vorticity, Reynolds stress, and velocity fluctuations, are highly affected by the variation of the Reynolds number. By the presence of horseshoe vortex system at $Z = F_s/9$ plane, the levels of these flow characteristics magnify and occupy wider area of flow field. Hence, activating these flow mechanisms can increase heat, mass, and momentum transfer near the plates, and vise versa.

Acknowledgement

The authors would like to acknowledge the financial support of office of Scientific Research Projects of Çukurova University for funding under contract No: AAP20025.

References

Akkoca, A., 2004. Computational modeling of turbulent heat transfer in plate fin and tube heat exchangers. PhD Thesis, Institute of Natural and Applied Sciences, Cukurova University, Department of Mechanical Engineering, Adana, Turkey, 230 p.

Ay, H., Jang, J.Y., Yeh, J.N., 2002. Local heat transfer measurements of plate finned-tube heat exchangers by infrared thermography. Int. J. Heat Mass Transfer 45, 4069–4078.

Critoph, R.E., Holland, M.K., Fisher, M., 1999. Comparison of steady state and trasnsient methods for measurement of local heat transfer in plate fin–tube heat exchangers using liquid crystal thermography with radiant heating. Int. J. Heat Mass Transfer 42, 1–12.

Goldstein, L.G., Sparrow, E.M., 1976. Experiments on the transfer characteristics of a corrugated fin and tube heat exchanger configuration. J. Heat Transfer, Trans. ASME (February), 26–32.

Halici, F., Taymaz, I., Gunduz, M., 2001. The effect of the number of tube rows on heat, mass, and momentum transfer in flat-plate finned tube heat exchangers. Energy 26, 963–972.

Jang, J.Y., Wu, M.C., Chang, W.J., 1996. Numerical and experimental studies of three-dimensional plate fin and tube heat exchangers. Int. J. Heat Mass Transfer 39 (14), 3057–3066.

Jang, Y.J., Lai, J.T., Liu, C.T., 1998. The thermal-hydraulic characteristics of staggered circular finned tube heat exchangers under dry and dehumidifying conditions. Int. J. Heat Mass Transfer 41, 3321–3337.

Kim, J.Y., Song, T.H., 2002. Microscopic phenomena and macroscopic evaluation of heat transfer from plate fins/circular tube assembly using naphthalene sublimation technique. Int. J. Heat Mass Transfer 45 (16), 3397–3404.

Kim, J.Y., Song, T.H., 2003. Effect of tube alignment an the heat/mass transfer from a plate fin and two-tube assembly: naphthalene sublimation results. Int. J. Heat Mass Transfer 46, 3051–3059.

Kundu, D., Skeikh, A.H., Lou, D.Y.S., 1992. Heat transfer in crossflow over cylinders between two parallel plates. Numer. Heat Transfer, Pt. A 114, 558–564.

Lozza, G., Merlo, U., 2001. An experimental investigation of heat transfer and friction losses of interrupted and wavy fins for fin-and-tube heat exchangers. Int. J. Refrig. 24, 409–416.

Madi, M.A., Johns, R.A., Heikal, M.R., 1998. Performance characteristics correlation for round tube and plate finned heat exchangers. Int. J. Refrig. 21 (7), 507–517.

Mendez, R.R., Sen, M., Yang, K.T., McClain, R., 2000. Effect of fin spacing on convection in a plate fin and tube heat exchanger. Int. J. Heat Mass Transfer 43, 39–51.

Rocha, L.A.O., Saboya, F.E.M., Vargas, J.V.C., 1997. A comparative study of elliptical and circular sections in one- and two-row tubes and plate fin heat exchangers. Int. J. Heat Fluid Flow 18, 247–252.

Saboya, F.E.M., Sparrow, E.M., 1974. Local and average transfer coefficients for one row plate fin and tube heat exchanger configurations. J. Heat Transfer, Trans. ASME. (August), 265–272.

Seshimo, Y., Fujii, M., 1991. An experimental study on the performance of plate fin and tube heat exchangers at low Reynolds numbers. ASME/JSME Thermal Eng. Proc. (4), 449–454.

Shah, R.K., Heikal, M.R., Thonon, B., 1997. Advances in numerical analysis of fluid flow, heat transfer, and flow friction characteristics of

compact heat exchanger surfaces. In: Proceedings, International Symposium on Fluid Flow and Heat Transfer, Ankara, Turkey, pp. 68–87.

Tutar, M., Akkoca, A., 2004. Numerical analysis of fluid flow and heat transfer characteristics in three dimensional plate fin and tube heat exchangers. Numer. Heat Transfer, Pt. A 46, 1–21.

Valencia, A., Fiebig, M., Mitra, N.K., 1996. Heat transfer enhancement by longitudinal vortices in a fin- tube heat exchanger element with flat tubes. J. Heat Transfer 118, 209–211.

Wang, C.C., Fu, W.L., Chang, C.T., 1997. Heat transfer and friction characteristics of typical wavy fin-and-tube heat exchangers. Exp. Thermal Fluid Sci. 14, 174–186.

Wang, C.C., Tsai, Y.M., Lu, D.C., 1998. Comprehensive study of convex-louver and wavy fin- and tube-heat exchangers. J. Thermophys. Heat Transfer 12 (3), 423–430.

Wang, C.C., Lin, Y.T., Lee, C.J., Chang, J.Y., 1999a. Investigation of wavy fin-and-tube heat exchangers: a contribution to databank. Exp. Heat Transfer 12, 73–89.

Wang, C.C., Chang, J.Y., Chiou, N.F., 1999b. Effects of waffle height on the air side performance of wavy fin-and-tube heat exchangers. Heat Transfer Eng. 20 (3), 45–56.

Wierbowski, M., Stasiek, J., 2002. Liquid Crystal Technique for Heat transfer Investigation in a fin–tube heat exchanger element. Exp. Thermal Fluid Sci. 26 (2–4), 319–323.

Yan, W.M., Sheen, P.J., 2000. Heat transfer and friction characteristics of fin and tube heat exchangers. Int. J. Heat Mass Transfer 43, 1651–1659.

Zdravitsch, F., Fletcher, C.A.J., Behnia, M., 1994. Laminar and turbulent heat transfer predictions in tube banks in cross flow. In: Proceedings, International Conference on Fluid and Thermal Energy Conversion, Indonesia, pp. 12–16.